INTERNATIONAL JOURNAL OF PRECISION ENGINEERING AND MANUFACTURING Vol. 16, No. 10, pp. 2147-2157 SEPTEMBER 2015 / 2147
DOI: 10.1007/s12541-015-0277-9 ISSN 2234-7593 (Print) / ISSN 2005-4602 (Online)

Theoretical and Experimental Investigations on Parallel-Axis Gear Transmission with Tubular Meshing Surfaces

Dong Liang[1,#], Bingkui Chen[1], and Yane Gao[1]

1 State Key Laboratory of Mechanical Transmission, Chongqing University, No.174, Shazhengjie, Shapingba, Chongqing, 400044, China
Corresponding Author / E-mail: liangdong213@cqu.edu.cn, TEL: +86-023-65106247, FAX: +86-023-65106247

KEYWORDS: Gear, Meshing successive property, Parametric design, Transmission efficiency, Tubular meshing surfaces

Theoretical and experimental investigations on parallel-axis gears with tubular meshing surfaces are performed in this study. Based on theory of conjugate curves, the parametric design for tubular tooth profiles is provided and solid models are established for motion simulation. Tubular meshing surfaces are evaluated according to geometric and meshing characteristics including undercutting condition, interference with engagement and curvature, calculation of sliding ratios, and successive meshing property. The meshing essence of tubular tooth surfaces is determined. The mechanics properties of tooth surfaces are analyzed using the finite element method. The contact stress, meshing law and deformation analysis of tooth surfaces are presented. The transmission efficiency experiment is based on the developed gear prototype, and a comparison of the prototype with an involute gear drive is provided. Further research on the dynamics analysis and key manufacturing technology will be conducted, and this gear drive is expected to exhibit excellent transmission performance.

Manuscript received: November 4, 2014 / Revised: July 11, 2015 / Accepted: July 13, 2015

1. Introduction

With the development of science and technology, the demand for high-performance gear transmission has gradually increased. Transmission properties have improved because numerous scholars have conducted related research on modifying gear tooth and have developed new materials and precision manufacturing technology.[1-6] In particular, the production of new types of gear drives plays an important role in practical engineering applications.[7-11]

Gear transmission with tubular meshing surfaces is a new type of spatial gear drive that can be used to transmit motion and power between two parallel or intersecting axes. This proposed gear drive is based on theory of conjugate curves instead of theory of conjugate surfaces.[12-15] Through the current research, the conjugated curve of a given contact curve in a plane or space coordinate system along a given contact direction is derived, and tubular meshing tooth surfaces can be generated based on the conjugate-curve pair.

In this study, theoretical and experimental investigations on parallel-axis gears with tubular meshing surfaces are performed. Based on the generation method and mathematical models, the parametric design for tooth profiles is provided. The general geometric features of tooth surfaces are discussed, and their contact characteristics are analyzed via the finite element method. The transmission efficiency experiment is based on the developed gear prototype. The summarized conclusions are provided in the final section of this paper.

2. Geometric Design of the Gear Pair

2.1 Generation method and mathematical models

Tubular tooth surfaces for a parallel-axis gear drive are generated based on the equidistant-enveloping method.[13] As shown in Fig. 1, the generation of tooth surfaces involves four steps.

Step 1: The solution to the conjugated curve in a given contact position for an arbitrary curve is developed according to theory of conjugate curves.

Step 2: Equidistant motion along the designated normal orientation is established for each conjugate-curve pair. Note that selecting movement direction and adjusting equidistance can affect the types of contact of tooth profiles.

Step 3: The enveloping surface of the family of spheres are generated according to sphere motion along the developed equidistant curve.

Step 4: Tooth profiles are determined based on a limited range from tip to root.

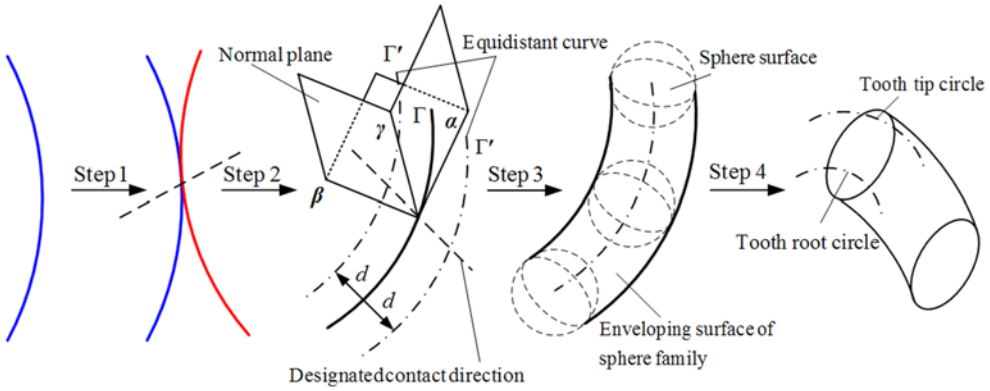

Fig. 1 Generation method of tubular tooth surfaces

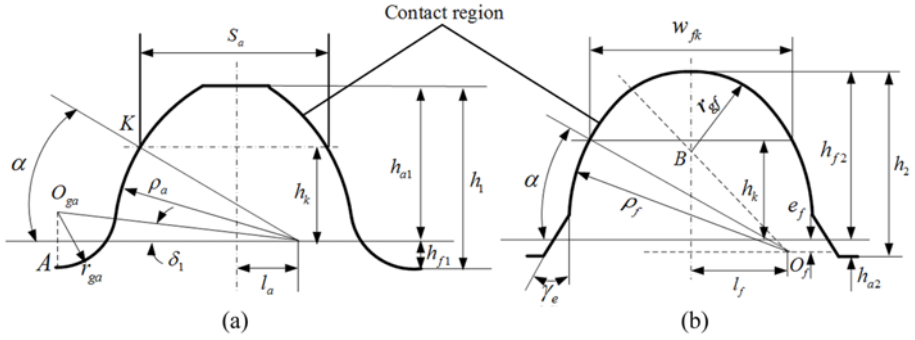

Fig. 2 Tooth profiles in normal section: (a) convex tooth profile and (b) concave tooth profile

Table 1 Design parameters of tubular tooth profiles

Parameters	Convex tooth	Concave tooth
α - Pressure angle	20~35°	20~35°
h_i (i=a, f) - Tooth height	1.5m_n	1.52m_n
h_{ai} (i=1, 2) - Tooth addendum height	1.2339m_n	0.1661m_n
h_{fi} (i= 1, 2) - Tooth dedendum height	0.2661m_n	1.3539m_n
ρ_i (i=a, f) - Radius of circular-arc tooth profile	1.5m_n	1.52m_n
e_i (i=a, f) - Movement distance of circle center	0	0.01m_n
l_i (i=a, f) - Offset distance of circle center	0.5895m_n	0.5596m_n
h_k - Distance between contact point and pitch curve	0.6339m_n	0.6339m_n
S_{ai} (i=a, f) - Tooth thickness in contact point	1.54m_n	1.54m_n
ω_{ik} (i=a, f) - Tooth space in contact point	1.6016m_n	1.5416m_n
j - Tooth crack	0	0.05m_n
r_{gi} (i=a, f) - Circle radius of tooth root	0.4m_n	0.452m_n
δ_l (i=a, f) - Process angle	4°2′31″	4°52′55″
γ_e - Addendum chamfer angle of concave tooth	none	45°
h_e - Addendum chamfer height of concave tooth	none	0.15m_n

*m_n represents the normal modulus.

2.2 Parametric design of tooth profiles

According to the aforementioned approach, the generated tubular tooth surfaces have contact advantages from the circular-arc tooth profile and the given conjugate-curve pair. The mating tooth profiles are designed by following Step 4. As shown in Fig. 2, the normal sections of the convex and concave tooth profiles are developed. This section contains three parts: the engagement region, the tooth fillet, and the tip/root limit. The basic parameters of tooth profiles are listed in Table 1.

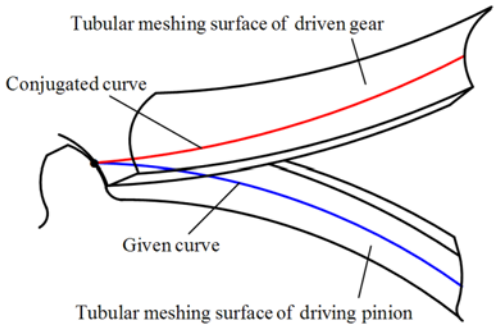

Fig. 3 Contact point of mating tooth profiles

For an arbitrary planar or spatial curve, the ideal contact condition can be achieved by simultaneously considering the conjugate-curve pair and the optional contact direction. As shown in Fig. 3, the tooth profiles come in contact with one another at a distinctive point, which is also the common tangent point. In this study, the single-point contact case is discussed and the multi-point contact case is investigated further.

2.3 Solid models

Based on the equations of tooth surfaces in Ref. 13, the computer program for calculating the data points of tooth surfaces is developed

Table 2 Parameters of gears with tubular meshing surfaces

Parameters	Values
r_1 - Radius of pitch circle of pinion (mm)	22
r_2 - Radius of pitch circle of gear r_2 (mm)	68
m_n - Module (mm)	4
Z_1 - Tooth number of pinion	11
Z_2 - Tooth number of gear	34
α - Pressure angle (°)	30
i_{21} - Transmission ratio	3.09
ρ_1 - Radius of tooth profile of pinion (mm)	4
ρ_2 - Radius of tooth profile of gear (mm)	4.4
p - Helix parameter	28.6478
d_1 - Equidistant distance of pinion (mm)	4
d_2 - Equidistant distance of gear (mm)	4.4
B - Tooth width (mm)	30
t - Range of curve parameter (rad)	0~1.05

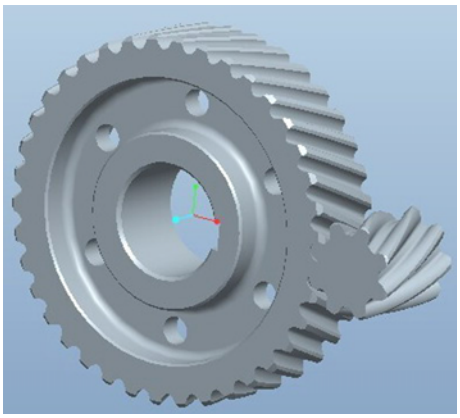

Fig. 4 Solid model of a gear pair

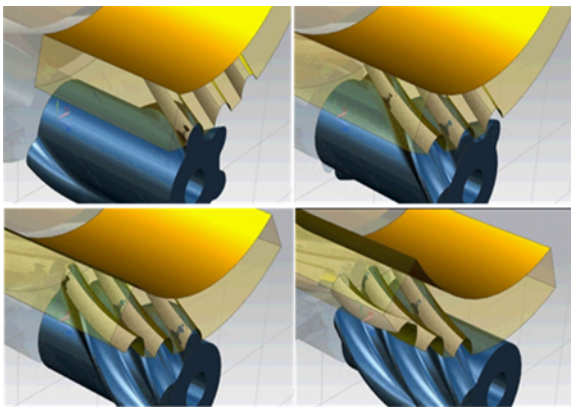

Fig. 5 Motion simulation of simplified models

in MATLAB. The results are exported to the 3D drawing software Pro/E according to the mathematical parameters given in Table 2. Tooth surfaces can be generated by surface function. Moreover, the solid models of gear pairs are established as shown in Fig. 4.

Based on the simplified models in Fig. 5, a computerized simulation of the meshing process is conducted to demonstrate the feasibility of this gear drive and evaluate its meshing and contact conditions. The following characteristics are observed: (1) The gears can transmit rotational motion with a constant gear ratio and fulfil continuous transmission between mating tooth surfaces. (2) Tooth surfaces come in contact along the conjugate curves in the axial direction, which is the ideal design condition. (3) No meshing interference is observed between couple tooth surfaces.

3. Geometric and Meshing Characteristics of Gear Pair

3.1 Undercutting of tooth surfaces

Tooth undercutting occurs when a singular point appears on a tooth surface. For gears with tubular tooth surfaces, the pinion is more sensitive to undercutting due to its less number of teeth. The approach proposed in Ref. 16 is used to analyze this problem. Using a single tooth flank as an example, the equation of the contact region can be expressed as follows

$$\begin{cases} x = -\rho_a \sin\alpha_a - e_a \\ y = -(\rho_a \cos\alpha_a - l_a)\cos\beta + u_a \sin\beta \\ z = (\rho_a \cos\alpha_a - l_a)\sin\beta + u_a \cos\beta \end{cases} \tag{1}$$

Where ρ_a is the radius of the convex circular-arc tooth profile, e_a is the movement distance of the circle center, l_a is the offset distance of the circle center. α_a represents the pressure angle, β indicates the helix angle, and u_a expresses the displacement of the tooth profile in the axial direction.

Suppose that surface Σ_1 is the tool surface in a two-parameter form, and it generates gear tooth surface Σ_2. The appearance of singular points on Σ_2 indicates that the surface may be undercut during the generation process. The mathematical definition of the singularity of Σ_2 may be represented by the equation $v_r^{(2)} = 0$, which yields $v_r^{(1)} + v^{(12)} = 0$, where $v_r^{(2)}$ and $v_r^{(1)}$ represent the relative velocity of the contact point over tooth surfaces S_1 and S_2, respectively. $v^{(12)}$ is the sliding velocity. Based on the meshing expression and differentiated equation of tubular tooth surfaces, we obtain

$$\frac{d}{ds}[\Phi(t, \varphi, \alpha)] = 0 \tag{2}$$

Where s is the introduced arc parameter, t is the curve parameter, and φ, α are the tubular meshing surface parameters. $\Phi(t, \varphi, \alpha)$ represents the enveloping conditions of tubular tooth surfaces, with $\Phi(t, \varphi, \alpha) \equiv (\boldsymbol{r}_t, \boldsymbol{r}_\varphi, \boldsymbol{r}_\alpha) = 0$. Thus, a line on surface Σ_1 that generates singular points on Σ_2 can be determined. According to gear geometry,[16] the following relationship can be derived:

$$\begin{cases} \dfrac{\partial r_1}{\partial t}\dfrac{dt}{ds} + \dfrac{\partial r_1}{\partial \varphi}\dfrac{d\varphi}{ds} = -v_1^{(12)} \\ \dfrac{\partial \Phi}{\partial t}\dfrac{dt}{ds} + \dfrac{\partial \Phi}{\partial \varphi}\dfrac{d\varphi}{ds} = -\dfrac{\partial \Phi}{\partial \alpha}\dfrac{d\alpha}{ds} \end{cases} \tag{3}$$

where, $\partial r_1/\partial t$, $\partial r_1/\partial \varphi$, and $v_1^{(12)}$ are three- or two-dimensional vectors for spatial and planar gearing, respectively. These vectors are represented in coordinate system S_1, which is connected to driving pinion 1 based on the principle of conjugate curves.[12] Eq. (3) expresses a system of four linear equations with two unknowns, i.e., dt/ds and

$d\varphi/ds$, whereas $d\alpha/ds$ is given. This system has a definite solution to the unknowns if the matrix

$$A=\begin{bmatrix}\frac{\partial r_1}{\partial t} & \frac{\partial r_1}{\partial \varphi} & -v_1^{(12)}\\ \frac{\partial \Phi}{\partial t} & \frac{\partial \Phi}{\partial \varphi} & -\frac{\partial \Phi}{\partial \alpha}\frac{d\alpha}{ds}\end{bmatrix} \tag{4}$$

has the rank $r=2$, which yields

$$\Delta_1=\begin{bmatrix}\frac{\partial x_1}{\partial t} & \frac{\partial x_1}{\partial \varphi} & -v_{x1}^{(12)}\\ \frac{\partial y_1}{\partial t} & \frac{\partial y_1}{\partial \varphi} & -v_{y1}^{(12)}\\ \frac{\partial \Phi}{\partial t} & \frac{\partial \Phi}{\partial \varphi} & -\frac{\partial \Phi}{\partial \alpha}\frac{d\alpha}{ds}\end{bmatrix};\quad \Delta_2=\begin{bmatrix}\frac{\partial x_1}{\partial t} & \frac{\partial x_1}{\partial \varphi} & -v_{x1}^{(12)}\\ \frac{\partial z_1}{\partial t} & \frac{\partial z_1}{\partial \varphi} & -v_{z1}^{(12)}\\ \frac{\partial \Phi}{\partial t} & \frac{\partial \Phi}{\partial \varphi} & -\frac{\partial \Phi}{\partial \alpha}\frac{d\alpha}{ds}\end{bmatrix};$$

$$\Delta_3=\begin{bmatrix}\frac{\partial y_1}{\partial t} & \frac{\partial y_1}{\partial \varphi} & -v_{y1}^{(12)}\\ \frac{\partial z_1}{\partial t} & \frac{\partial z_1}{\partial \varphi} & -v_{z1}^{(12)}\\ \frac{\partial \Phi}{\partial t} & \frac{\partial \Phi}{\partial \varphi} & -\frac{\partial \Phi}{\partial \alpha}\frac{d\alpha}{ds}\end{bmatrix};\quad \Delta_1=\begin{bmatrix}\frac{\partial x_1}{\partial t} & \frac{\partial x_1}{\partial \varphi} & -v_{x1}^{(12)}\\ \frac{\partial y_1}{\partial t} & \frac{\partial y_1}{\partial \varphi} & -v_{y1}^{(12)}\\ \frac{\partial z_1}{\partial t} & \frac{\partial z_1}{\partial \varphi} & -v_{z1}^{(12)}\end{bmatrix}.$$

where $v_{x1}^{(12)}$, $v_{y1}^{(12)}$ and $v_{z1}^{(12)}$ are the coordinate components of velocity vector $v_1^{(12)}$ in coordinate system S_1. Based on the simplified process for Δ_4, it is the same as the meshing equation and is satisfied because the tangency points of surfaces Σ_1 and Σ_2 are considered. Only Δ_1, Δ_2 and Δ_3 should be applied to determine singularity conditions for the generated tooth surface Σ_2. Furthermore, a sufficient condition for the singularity of Σ_2 can be represented by

$$\Delta_1^2+\Delta_2^2+\Delta_3^2=F(t,\varphi,\alpha)=0 \tag{5}$$

By substituting Eq. (1) into the preceding equations, the undercutting condition of tubular tooth surfaces is obtained as follows:

$$\begin{aligned}\Delta_1=&-\rho_a\cos\alpha_a\sin\beta\frac{\partial\Phi}{\partial\alpha}-(-r_1\varphi_1+y)\rho_a\sin\alpha_a\cos\beta\frac{\partial\Phi}{\partial\varphi}\\&+(-r_1\varphi_1+y)\frac{\partial\Phi}{\partial t}\sin\beta+(z-x)\rho_a\sin\alpha_a\frac{\partial\Phi}{\partial\varphi}=0\end{aligned} \tag{6}$$

$$\begin{aligned}\Delta_2=&(-r_1\varphi_1+y)\rho_a\sin\alpha_a\sin\beta\frac{\partial\Phi}{\partial\varphi}-\rho_a\cos\alpha_a\cos\beta\frac{\partial\Phi}{\partial\alpha}\\&+(-r_1\varphi_1+y)\cos\beta\frac{\partial\Phi}{\partial t}+(-r_1\varphi_1+y)\rho_a\cos\alpha_a\frac{\partial\Phi}{\partial\varphi}=0\end{aligned} \tag{7}$$

$$\begin{aligned}\Delta_3=&(z-x)\rho_a\sin\alpha_a\sin\beta\frac{\partial\Phi}{\partial\varphi}+\rho_a\sin\alpha_a\cos\beta\frac{\partial\Phi}{\partial\alpha}\\&+(-r_1\varphi_1+y)\sin\beta\frac{\partial\Phi}{\partial t}+(z-x)\cos\beta\frac{\partial\Phi}{\partial t}\\&+(-r_1\varphi_1+y)\rho_a\sin\alpha_a\cos\beta\frac{\partial\Phi}{\partial\varphi}=0\end{aligned} \tag{8}$$

where

$$\varphi_1=\frac{1}{r_1}\left[\frac{\cos\alpha\cos\beta(x+z)}{\sin\alpha+\cos\alpha\sin\beta}+y\right]$$

$$\frac{\partial\Phi}{\partial\alpha}=-r_1(\sin\alpha+\cos\alpha\sin\beta)$$

$$\frac{\partial\Phi}{\partial\varphi}=\sin\alpha\sin\beta+\cos\alpha$$

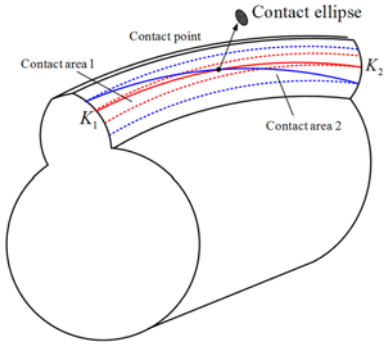

Fig. 6 Contact area of tooth surface

$$\begin{aligned}\frac{\partial\Phi}{\partial t}=&\rho\sin\alpha\cos\beta(\sin\alpha+\cos\alpha\sin\beta)+(x+z)\sin\alpha\cos\beta\\&+(\cos\alpha-\sin\alpha\sin\beta)(-r_1\varphi_1+y+\rho\cos\alpha\sin\beta)\end{aligned}$$

A simple approach to avoid singularity and undercutting of a generated surface is through the following expression:

$$\begin{cases}r_1=r_1(t,\varphi)\\ \Phi(t,\varphi,\alpha)=0\\ F(t,\varphi,\alpha)=0\end{cases} \tag{9}$$

The equations determine a line that limits the generation of surface Σ_1. In many cases, the undercutting can be avoided by choosing appropriate settings for surface Σ_1 that generates Σ_2.

3.2 Interference analysis of tooth surfaces

The working region of tooth profiles should only contain the regular point. Normal and tangent planes are uncertain at a singular point, which can cause interference.

3.2.1 Meshing interference

The contact point along a pair of conjugate curves on two tubular tooth surfaces was described in a previous study. In kinematics, conjugate curves can achieve continuous movement and fixed transmission ratio. In practice, however, two conjugate curves cannot satisfy the requirement for transmitting motion or power. Hence, transformation from the curve to the surface is developed by considering the proposed equidistant-enveloping method. Based on the design requirement, arbitrary curves may be selected as conjugate curves when these are limited within the variable range.

The contact area in the axial direction is shown in Fig. 6. The two tooth surfaces are engaged in point contact during the initial stage; however, the contact point gradually becomes the contact ellipse during the meshing process. The load capacity of this gear drive can be improved because of the larger contact area between two tooth surfaces. If a different curve range is given under the conditions of a designated contact, then the tooth surfaces with a larger contact area can show better transmission characteristics.

If the difference in curvature radii between the pinion and the gear is small, then meshing interference may occur. Assuming that two mating gears mesh in point P and Δk is described as the interference value in Fig. 7, then the tubular tooth profiles are not in their correct contact positions. The tooth profiles intersect with each other at points

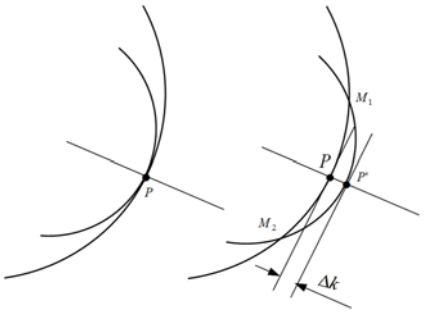

Fig. 7 Meshing interference

M_1 and M_2. P' is the maximum distance point, and distance Δk between points P and P' is represented as

$$\Delta k = \sqrt{(x_k - x_{k'})^2 + (y_k - y_{k'})^2} \tag{10}$$

3.2.2 Curvature interference

The induced normal curvature K_{12} ($K_{12}=K_1-K_2$) of tubular tooth surfaces can be calculated based on gear geometry and its applied theory. Given the orientation of common normal ***n*** from an entity to an empty space at contact point P, tooth surfaces mesh normally only if the K_{12} value is negative, whereas curvature interference may occurs if the K_{12} value is positive.[17] Fig. 8 shows the general form of four kinds of tubular tooth profiles: convex-to-convex, concave-to-concave, convex-to-concave, and concave-to-convex.

(a) $K_1 < 0$ and $K_2 > 0$. K_{12} is negative. The bending directions of tooth profiles are different and no curvature interference occurs.

(b) $K_1 > 0$ and $K_2 < 0$. The bending directions of tooth profiles are different. K_{12} is positive, and curvature interference will occur.

(c) $K_1<0$ and $K_2<0$. The bending directions of tooth profiles are the same. If $|K_1| > |K_2|$, then K_{12} is negative and no curvature interference occurs. If $|K_1| < |K_2|$, then K_{12} is positive and curvature interference will occur.

(d) $K_1>0$ and $K_2>0$. The bending directions of tooth profiles are the same. If $K_1 < K_2$, then K_{12} is negative and no curvature interference occurs. If $K_1 > K_2$, then K_{12} is positive and curvature interference will occur.

Hence, the induced normal curvature K_{12} of tubular meshing surfaces must be negative to prevent curvature interference from occurring.

3.3 Sliding ratios of tooth surfaces

The general calculation method for the sliding ratios of tubular tooth surfaces is studied in terms of the derived conjugate curves. Suppose a driving gear with original curve Γ_1 transmits movement to a driven gear with its conjugated curve Γ_2, the gears will be in contact at point K, as shown in Fig. 9. ΔS_1 and ΔS_2 denote the travelling arcs of conjugate curves Γ_1 and Γ_2, respectively, in time Δt, which approaches zero during the meshing process. Assuming that relative sliding occurs, the length of arc KK_1 is unequal to that of arc KK_2, and the difference between ΔS_1 and ΔS_2 is called the sliding arc. The sliding coefficient is analyzed as a ratio of the length of the sliding arc relative to the length of the corresponding arc in the meshing area.

The formulas for calculating the sliding ratios of a gear pair can be

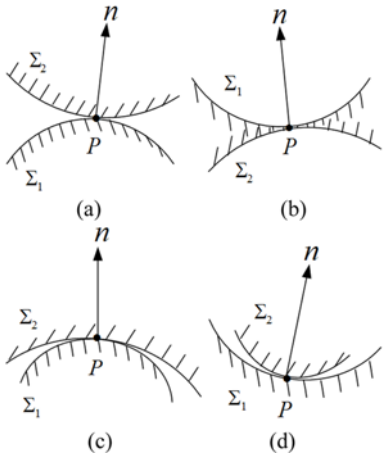

Fig. 8 Curvature interference

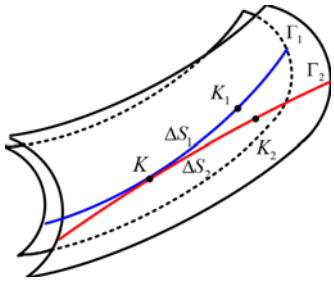

Fig. 9 Sliding condition of tooth surfaces

expressed as follows:

$$\eta_1 = \lim_{\Delta S_1 \to 0} \frac{\Delta S_1 - \Delta S_2}{\Delta S_1} = \frac{\frac{dS_1}{dt} - \frac{dS_2}{dt}}{\frac{dS_1}{dt}} = \frac{dS_1 - dS_2}{dS_1} \tag{11}$$

and

$$\eta_2 = \lim_{\Delta S_2 \to 0} \frac{\Delta S_2 - \Delta S_1}{\Delta S_2} = \frac{\frac{dS_2}{dt} - \frac{dS_1}{dt}}{\frac{dS_2}{dt}} = \frac{dS_2 - dS_1}{dS_2} \tag{12}$$

where

$$dS_1 = \sqrt{dx_1^2 + dy_1^2 + dz_1^2}\,dt$$

$$dS_2 = \sqrt{dx_2^2 + dy_2^2 + dz_2^2}\,dt$$

The parametric forms of conjugate curves Γ_1 and Γ_2 are represented in Ref. 12. Thus, we have

$$\begin{cases} \frac{dx_1}{dt} = x_1'(t) \\ \frac{dy_1}{dt} = y_1'(t) \\ \frac{dz_1}{dt} = z_1'(t) \end{cases} \tag{13}$$

and

$$\begin{cases} \dfrac{dx_2}{dt} = c'_{2t}x_1(t)+c_2x'_1(t)-c'_{1t}y_1(t)-c_1y'_1(t)+ai_{21}\phi'_{1t}\sin(i_{21}\phi_1) \\ \dfrac{dy_2}{dt} = c'_{1t}x_1(t)+c_1x'_1(t)+c'_{2t}y_1(t)+c_2y'_1(t)-ai_{21}\phi'_{1t}\cos(i_{21}\phi_1) \\ \dfrac{dz_2}{dt} = z'_1(t) \end{cases} \quad (14)$$

where

$$c_1 = \sin[(1+i_{21})\phi_1],\ c_2 = \cos[(1+i_{21})\phi_1],$$

$$c'_{1t} = (1+i_{21})\phi'_{1t}c_2,\ c'_{2t} = -(1+i_{21})\phi'_{1t}c_1,$$

$$\phi'_{1t} = \frac{1}{\sqrt{1-\dfrac{M^2}{E^2+F^2}}}\left(\frac{M}{\sqrt{E^2+F^2}}\right)' + \frac{1}{1+\left(\dfrac{E}{F}\right)^2}\left(\frac{E}{F}\right)'$$

where a is the central distance. Symbols E, F and M are expressed in Ref. 12. After substituting Eqs. (13) and (14) into the formulas, the sliding ratios of the gear pair with tubular tooth surfaces can be obtained. This method is suitable for arbitrary conjugate tooth profiles that come in contact along a specific locus in the axial direction. Deriving complicated geometric relationships for calculation is unnecessary.

3.4 Conjugate successive characteristic

The meshing of tooth profiles is only described as the point contact in the axial orientation between convex and concave tooth surfaces. The accurate description of the meshing process is not clearly provided. Thus, the meshing essence of tooth surfaces is demonstrated in this section.

Based on theory of conjugate curves,[12,13] the equations of tooth surfaces Σ_1 and Σ_2 can be represented in a fixed coordinate system $S(O\text{-}x, y, z)$. When two gears mesh in an arbitrary contact point, the correlation function can be obtained as follows:

$$\begin{cases} x_{\Sigma1}\cos\phi_1 - y_{\Sigma1}\sin\phi_1 - (x_{\Sigma2}-a)\cos(i_{21}\phi_1) + y_{\Sigma2}\sin(i_{21}\phi_1) = 0 \\ x_{\Sigma1}\sin\phi_1 + y_{\Sigma1}\cos\phi_1 - (x_{\Sigma2}-a)\sin(i_{21}\phi_1) - y_{\Sigma2}\cos(i_{21}\phi_1) = 0 \\ z_{\Sigma1} - z_{\Sigma2} = 0 \end{cases} \quad (15)$$

where ϕ_1 is a function with respect to parameter t that is derived by the meshing equation. Based on the expression $z_1 - z_2 = 0$, the relationship between parameters t and α is expressed as follows:

$$\alpha = \arcsin\frac{(z_{hz1}-z_{hz2})T_2 \pm \sqrt{T_1^4 + T_1^2T_2^2 - T_1^2(z_{hz1}-z_{hz2})^2}}{T_1^2+T_2^2} \quad (16)$$

where $z_{hzi} = z_i + d_in_i^0$ $(i = 1, 2)$, d_i is the equidistance, and n_i^0 is the unit normal under different coordinate systems. The unit normal has $T_1 = \dfrac{d_1^2x'_{hx1}}{z'_{hz1}} - \dfrac{d_2^2x'_{hx2}}{z'_{hz2}}$; $T_2 = \dfrac{d_1^2y'_{ht1}}{z'_{hz1}} - \dfrac{d_2^2y'_{hy2}}{z'_{hz2}}$.

The following expression is obtained after substituting Eq. (16) into Eq. (15):

$$\begin{aligned} &x_{\Sigma1}^2 + y_{\Sigma1}^2 + (x_{\Sigma2}-a)^2 + y_{\Sigma2}^2 + 2(y_{\Sigma1}-x_{\Sigma1}y_{\Sigma2})\sin(\phi_1 - i_{21}\phi_1) \\ &-2[x_{\Sigma1}(x_{\Sigma2}-a) + y_{\Sigma1}y_{\Sigma2}]\cos(\phi_1 - i_{21}\phi_1) = 0 \end{aligned} \quad (17)$$

Only parameter t is indicated in the formula, and the arbitrary meshing point can be calculated by solving the equation. The differential equations of the tooth surfaces of the pinion and the gear with respect to parameters t and α are represented as follows:

$$\begin{cases} x_{\Sigma it} = x'_i \pm d_in^0_{nxi}{}' + d_i\phi_t\sin\varphi\cos\alpha \\ y_{\Sigma it} = y'_i \pm d_in^0_{nyi}{}' + d_i\phi_t\sin\varphi\sin\alpha \\ z_{\Sigma it} = z'_i \pm d_in^0_{nzi}{}' + d_i\phi_t\cos\varphi \end{cases} \quad (i = 1,2) \quad (18)$$

and

$$\begin{cases} x_{\Sigma i\alpha} = -d_i\phi_\alpha\sin\varphi\cos\alpha - d_i\cos\varphi\sin\alpha \\ y_{\Sigma i\alpha} = -d_i\phi_\alpha\sin\varphi\sin\alpha + d_i\cos\varphi\cos\alpha \\ z_{\Sigma i\alpha} = d_i\phi_\alpha\cos\varphi \end{cases} \quad (i = 1,2) \quad (19)$$

The normal vector of the tubular meshing surfaces at the contact point can be expressed as follows:

$$\begin{aligned} \boldsymbol{n} = &\left[(x'_1 \pm d_1n^0_{nx1}{}')d_1\phi_{\alpha_0}\cos\alpha - \frac{Dd_1^2\phi_{\alpha_0}\phi_{t_0}}{\sqrt{1+D^2}}\sin\alpha\left(\cos\alpha + \frac{1}{\sqrt{1+D^2}}\right)\right. \\ &\left. + d_1(z'_1 \pm d_1n^0_{nz1}{}')\frac{D\sin\alpha\phi_{\alpha_0} - \cos\alpha}{\sqrt{1+D^2}} - \frac{\cos\alpha d_1^2\phi_{t_0}}{1+D^2}\right]\boldsymbol{i} \\ &-\left[\frac{(x'_1 \pm d_1n^0_{nx1}{}')d_1\phi_{\alpha_0} + (z'_1 \pm d_1n^0_{nz1}{}')d_1(\phi_{\alpha_0}D\cos\alpha - \sin\alpha)}{\sqrt{1+D^2}}\right. \\ &\left. - \frac{d_1^2\sin\alpha\phi_{t_0}}{1+D^2}\right]\boldsymbol{j} + \left[\frac{(x'_1 \pm d_1n^0_{nx1}{}')d_1(\cos\alpha - D\sin\alpha\phi_{\alpha_0})}{\sqrt{1+D^2}}\right. \\ &\left. + \frac{(y'_1 \pm d_1n^0_{ny1}{}')d_1(D\phi_{\alpha_0}\cos\alpha + \sin\alpha) - Dd_1^2\phi_{t_0}\cos\phi}{\sqrt{1+D^2}}\right]\boldsymbol{k} \end{aligned} \quad (20)$$

where

$$\phi_{\alpha_0} = \frac{x'_1\sin\alpha - y'_1\cos\alpha}{(1+D^2)z'_{d1}}$$

$$\phi_{t_0} = \frac{(-x''_1\cos\alpha - y''_1\sin\alpha)z'_1 + (x'_1\cos\alpha + y'_1\sin\alpha)z''_1}{(1+D^2)z'_1}$$

$$D = \frac{-x'_1\cos\alpha - y'_1\sin\alpha}{z'_1}$$

According to the operation function of MATLAB, the simplified result is obtained and the components under the coordinate system are written as follows:

$$\begin{cases} n_x = \sin\alpha n_{\beta x1} + \cos\alpha n_{\gamma x1} \\ n_y = \sin\alpha n_{\beta y1} + \cos\alpha n_{\gamma y1} \\ n_z = \sin\alpha n_{\beta z1} + \cos\alpha n_{\gamma z1} \end{cases} \quad (21)$$

Based on the curve trihedron established in a contact point, the normal vector of the conjugate curves in the direction of the given contact position can be expressed as $n_n = \beta\sin\alpha + \gamma\cos\alpha$.[12] The result of the analysis of two expressions indicate that the normal vector at the contact point between two tubular meshing surfaces is the same as that of two conjugate curves.

The trajectory of contact motion consists of meshing points. The contact curves of different tooth surfaces can be developed by substituting the meshing points into the tooth surface equations. Considering coordinate transformation, the equations of contact locus curves are deduced and are determined to be the same as those of the conjugate curves designed in Ref. 12. As shown in Fig. 10, only a pair of curves

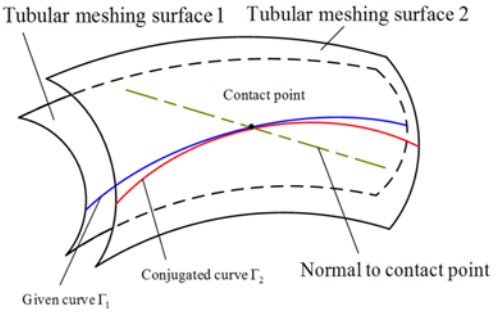

Fig. 10 Normal vector for tubular meshing surfaces and conjugate curves

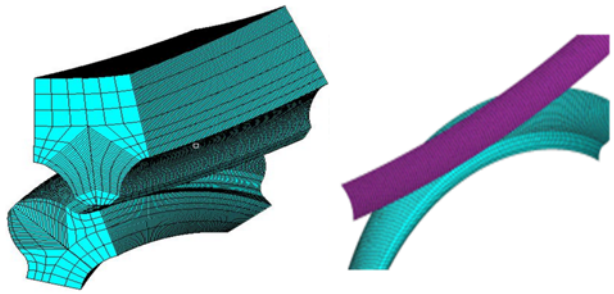

Fig. 12 Finite element model of the engagement pair: (a) network form and (b) meshing pair definition

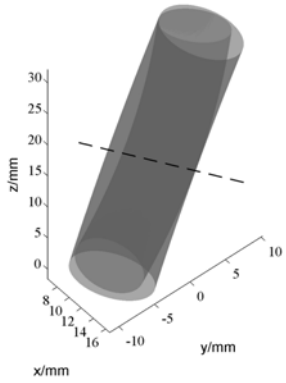

(a)

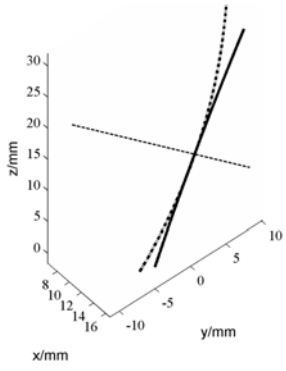

(b)

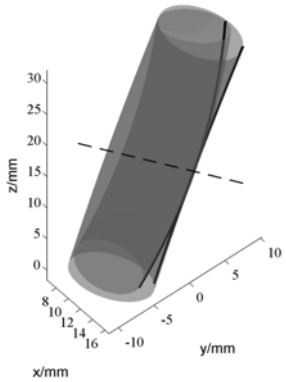

(c)

Fig. 11 Conjugate successive characteristic: (a) normal to tubular meshing surfaces, (b) normal to conjugate curves, (c) comparison of normal and contact locus

is in continuous and tangent contact during motion, and the transmission process contains the meshing characteristics of conjugate curves. The engagement in axial orientation between tubular tooth profiles has the same normal vector as that of the conjugate curves at the contact point.

A mathematical example is introduced to analyze the results. The theoretical model shown in Fig. 11 is designed based on the parameters in Table 2. Fig. 11(a) shows the normal vector of tubular meshing surfaces at a certain point (16.15 mm, 1.883 mm, 15.71 mm), and the normal vector for conjugate curves at the same point is described in Fig. 11(b). The comparison of the normal vector of both meshing pairs indicates that these conditions are coincident. Moreover, the contact locus on tubular meshing surfaces is also the conjugate-curve pair.

4. Analysis of Mechanics Property

In this section, the mechanics properties of the gear pair are discussed, and the condition of contact stress is analyzed using ANSYS. To obtain the optimal results for contact position, the single tooth model is utilized to carry out this study.

The pre-processing of the finite element analysis is conducted using Hypermesh software. For efficiency and accuracy, the element of the gear tooth is plotted with a low hexahedron unit Solid185. Stress convergence in the contact area and varying data ranges result in the dense plotting of the network. The unit size of the contact area is set to 0.2 mm, and the size in the no-contact area is set to 3 mm. The finite element model of the engagement pair is shown in Fig. 12. Based on the principle of meshing pair in ANSYS, the tooth surface of the pinion is regarded as the contact surface. The contact unit is defined as CONTA173, which means the low order quadrilateral element for 3D and 4-node. The tooth surface of the gear is considered the target surface, i.e., TARGE170. It means the shape of the target surface can be described by the various geometric forms under 3D condition. The sliding friction coefficient is set to 0.08 because of the well-lubricated condition between the pair of tooth surfaces.

The Hertz contact model is established to disregard the effect of friction on contact stress. The entire analysis process is examined based on the extended Lagrange algorithm. In general, an engagement action is considered standard, and contact FKN in the normal section is set to 1. To determine rotation and the given torque, a multi-point constraint unit (MPC184) is applied to this process. MPC184 corresponds to the

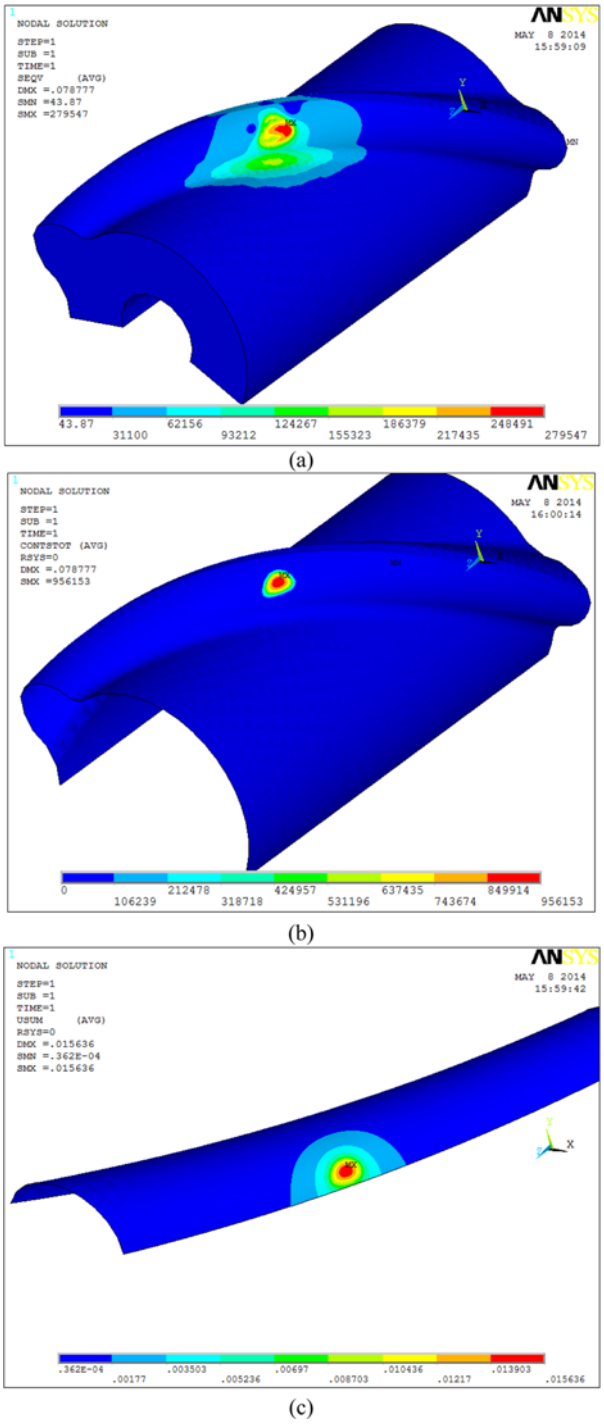

Fig. 13 Results of the finite element analysis of gears with tubular meshing surfaces: (a) equivalent stress, (b) contact stress, and (c) contact deformation

multi-rigidity beam connection between the rational central point and constraint surface. The entire material is 20CrMnTi with the properties $\nu = 0.25$, $E = 207$ GPa.

The pin connection is introduced into the meshing pair. Suppose that the gear is fixed and the torque applied to the pinion is 200 Nm, if unit MPC184 and the center of the pinion are considered as a whole, the multi-point constraint is established. The inner surface unit of the gear and its rotational center are fixed and applied to the entire

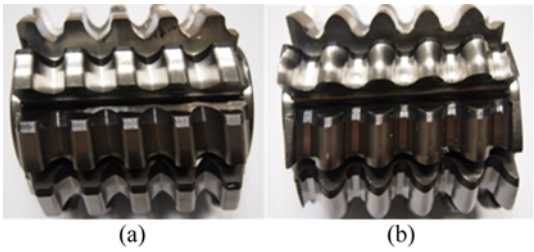

Fig. 14 Hobbing cutters for the gear pair: (a) hobbing for the pinion and (b) hobbing for the gear

constraint. Static analysis for the pinion in the middle of the tooth width is conducted, and the results are shown in Fig. 13. The stress unit is kPa and the length unit is mm.

As indicated in the equivalent stress graph in Fig. 13(a), stress concentration on the tooth root is not serious because of the circular arc fillet. The maximum bending stress is less than 280 MPa. The forces in the radial and axial directions are different, and the force in the axial direction is larger than that in the radial direction. The characteristics of the point contact is shown in Fig. 13(b). The maximum contact stress is approximately 956 MPa and can be reduced to the designated pressure angle. The form of the contact area is an ellipse, and the long half-axis is distributed along the axial orientation, which is consistent with the ideal condition. The contact deformation is illustrated in Fig. 13(c).

Involute gearing has extensive applications because it is easy to manufacture and shows mesh in line contact, constant meshing angle, and insensitivity to central distance variation. To analyze further the mechanics characteristics of parallel-axis gears with tubular meshing surfaces and to extend their applications in engineering, the comparisons of the proposed gear with involute gear drive will be carried out.

5. Performance Experiment

5.1 Prototype manufacturing

The gears are processed with hobbing cutters to achieve manufacturing precision. The hobs generated by rack cutters are designed and manufactured based on tubular tooth profiles. The hob products for convex pinion and concave gear are shown in Figs. 14(a) and 14(b), respectively.

Hobbing trials have been conducted using YS3140CNC hobbing machine controlled by the SIEMENS 840D system. It has good transmission stability, working accuracy and operability. Generation of the gear includes four movements: the rotation of the workpiece on its axis, the rotation of the hobbing cutter on its axis, and the feed motions of the hobbing cutter in the radial and axial directions. The rotational angles of the gear and hobbing cutter are represented by ϕ_g and ϕ_h, respectively. Hence, the following equation is obtained: $\phi_h/\phi_g = Z_g/N_h$, where Z_g is the number of gear teeth and N_h is the number of hob threads. The velocities of feed motions $\boldsymbol{v}_r$ and $\boldsymbol{v}_a$ are related as follows: $|v_r|/|v_a|=\tan\delta$, where δ is the setting angle of the hobbing cutter.

The processing of the pinion and gear is shown in Figs. 15(a) and 15(b), respectively. The final accuracy of the gear pair satisfies the

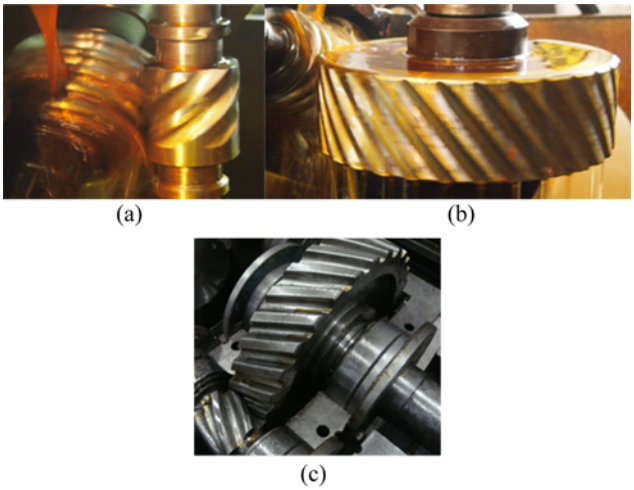

Fig. 15 Processing of the gear pair: (a) pinion, (b) gear, and (c) gear prototype

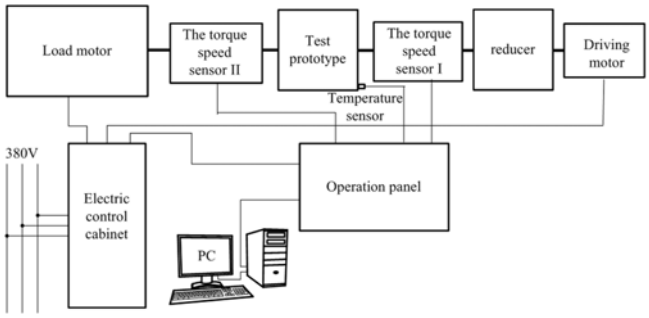

Fig. 16 Layout of the transmission performance test-bed

Table 3 Performance parameters of equipment

Equipment	Model number	Performance parameters
Prototype	CW100-63	Center distance: 144 mm Gear ratio: 5
Driving motor	YVPCG250M1-50	Power: 55 kW Speed: 0~4500 rpm
Loading motor	YVPCG315M3-16.7	Power: 55 kW Torque: 0~1051 Nm
Torque and rotational speed transducer I	JC1A	Nominal torque: 50 Nm
Torque and rotational speed transducer II	NJ2A	Nominal torque: 2000 Nm
Temperature transducer	WZP PT100	Range: -200~600°C

design requirements based on measuring instrument. The completed gear prototype is shown in Fig. 15(c).

5.2 Performance experiment

The transmission properties of the reducer prototype are evaluated. The layout of the test system is considered to investigate operational characteristics, as shown in Fig. 16. The equipment units are linked by spring coupling. Input and output powers are measured by the torque and rotational speed transducer. The oil temperature in the box is measured by the temperature transducer. Rotational speed is controlled by the variable speed electric motor, and the gear pair is loaded by the loading motor. The performance parameters of the equipment units are listed in Table 3 and the trial site is shown in Fig. 17.

Fig. 17 Testing site

The contact point between the conjugate tooth profiles will spread over a small area under a load because of elastic deformations. Hence, contact condition is localized. In general, when the contact area is large, the load capacities of the gear drive are high. To improve performance, conducting the running-in process is necessary. The contact area may be expanded to increase the load capability and gear tooth surfaces may be modified to reduce noise and vibration. The entire process is divided into five periods. Period one, which occurs after 2 hours of idle time, runs with an input shaft speed of 1250 rpm. It is followed by the second period with 2 hours of operation under a load (in this case, the output torque is 300 Nm). The third period lasts for 2 hours under a load (in this case, the output torque is 400 Nm). The fourth period also lasts for 2 hours under a load (in this case, the output torque is 500 Nm), and the last period occurs for another 2 hours under a load (in this case, the output torque is 600 Nm). After the running-in period, the ideal contact condition is achieved.

Input torque T_i and input shaft speed n_i can be measured by the torque and rotational speed transducer I, whereas output values T_o and shaft speed n_o can be measured by the torque and rotational speed transducer II. Transmission efficiency can be calculated as $\eta = n_o T_o / n_i T_i$. The speed values measured during the test are 500, 750, 1000, and 1250 r/min. The loads applied to tooth surfaces are 300, 400, 500, and 600 Nm. The oil temperature at each stage is also recorded.

Transmission efficiency under different operating conditions is shown in Fig. 18. Based on the results, transmission efficiency increases with rotational speed when torque is constant. Similarly, transmission efficiency increases with torque when rotational speed is constant. Maximum efficiency may reach 96.9% at a load of 600 Nm, and the efficiency of the entire prototype is 91.8~96.9%. Oil temperature is balanced when time is 60~70 min, and its optimal value is approximately 65.6°C.

The proposed gear drive is compared with a conventional involute gear drive under the same conditions. The results are shown in Fig. 19. Compared with the involute gear drive, the transmission efficiency of the proposed gear drive is lower. This observation is attributed to two reasons: (1) The mating gear pair is processed with the designed hobbing

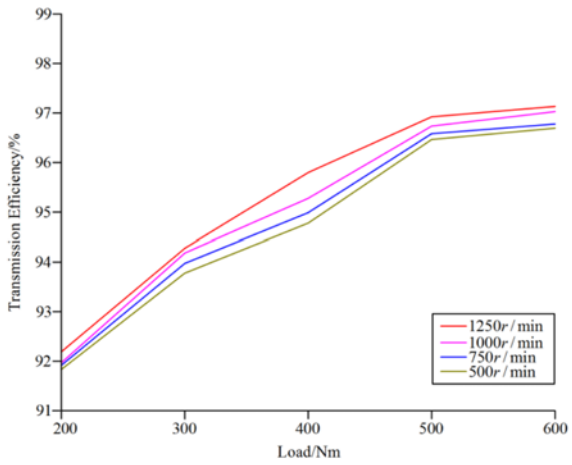

Fig. 18 Transmission efficiency of the proposed gears

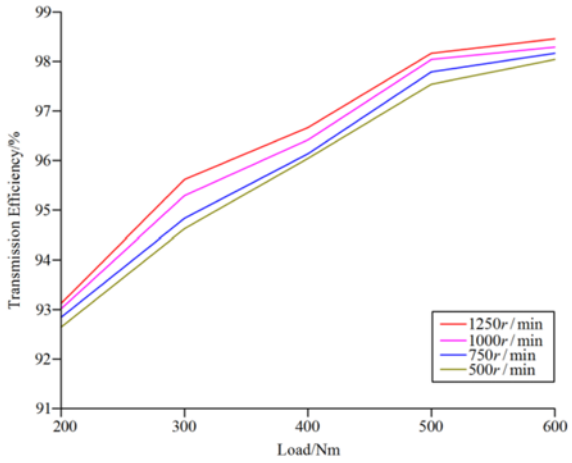

Fig. 19 Transmission efficiency of involute gears

cutters. Tooth surfaces are only generated by the rough hob cutting process; hence, the required precision is not achieved. (2) Machine and assembly errors in the gear drive may have a lower actual contact area than the theoretical contact area. In addition, sliding loss between mating tooth surfaces occurs. A vibration test of the parallel-axis gears with tubular meshing surfaces will be further carried out.

Three main problems that affect transmission performance occur in the conventional gear drive. (1) The high overload requirements in existing conjugate surfaces are difficult to satisfy. (2) Contact between convex and convex tooth profiles is common for contact patterns and has low strength. (3) A large sliding loss between general tooth surfaces can reduce transmission efficiency.

Compared with existing gear geometry, conjugate curves are more flexible and diverse in gear design and generation. Based on theory of conjugate curves, parallel-axis gears with tubular meshing surfaces are expected to have excellent transmission advantages: (1) Few teeth and a large module may be obtained without tooth undercutting. This feature can reduce the required installation space and help achieve the lightweight design. Meanwhile, bending strength will be enhanced. (2) The special meshing of generated convex and concave tooth profiles extends the relative radius of the curvature of the contact point and increases contact strength. Load capacity and usage life significantly improve. (3) Tooth surfaces mesh at a point contact along the conjugate curves and contain the transmission properties of conjugate curves. The approximate pure rolling contact between mating tooth surfaces may occur.

6. Conclusions

(1) The parametric design of tubular meshing surfaces is proposed based on the generation principle and mathematical models. According to the established solid models of gear pair, motion simulation is performed and the results are consistent with the design expectations.

(2) According to the analyses of geometric and meshing characteristics, undercutting of mating tooth surfaces is provided and interference analyses including engagement and curvature aspects are introduced. Based on a conjugate-curve pair, a calculation method for the sliding ratios of tubular meshing surfaces is presented. Meshing successive property is demonstrated, which presents the meshing essence of tubular tooth surfaces.

(3) Mechanics property of tubular meshing surface is analyzed based on the single tooth model. Stress concentration on the tooth root is insignificant because of the circular arc fillet, and the maximum bending stress is less than 280 MPa. The maximum contact stress is 956 MPa and can be reduced by decreasing the designated pressure angle. Point contact characteristic is also presented. The contact area resembles an ellipse, and the long half-axis is distributed along the axial orientation.

(4) The pinion and the gear are manufactured using the designed hobbing cutters. An efficiency experiment of the gear prototype is performed. Maximum efficiency may reach 96.9% with a load of 600 Nm and the efficiency of the entire prototype is 91.8~96.9%. The change in rotational speed is directly proportional with torque. Manufacturing precision and assembly error reduce efficiency.

(5) Further research on dynamic analysis and key manufacturing technology will be carried out. The proposed gear drive is expected to exhibit excellent transmission performance.

ACKNOWLEDGEMENT

This research was supported by National Science & Technology Pillar Program during the 12th Five-Year Plan Period of China (Grant No. 2013BAF01B04), and National Natural Science Foundation of China (Grant No. 51205425). The authors would like thank editor and reviewers for their helpful comments and suggestions to improve the manuscript.

REFERENCES

1. Zhang, H., Hua, L., and Han, X., “Computerized Design and Simulation of Meshing of Modified Double Circular-Arc Helical Gears by Tooth end Relief with Helix,” Mechanism and Machine Theory, Vol. 45, No. 1, pp. 46-64, 2010.

2. Wei, J., Zhang, Q., Xu, Z., and Lyu, S., "Study on Precision Grinding of Screw Rotors using CBN Wheel," Int. J. Precis. Eng. Manuf., Vol. 11, No. 5, pp. 651-658, 2010.

3. Jywe, W., Hsu, T.-H., and Liu, C.-H., "Non-Bar, an Optical Calibration System for Five-Axis CNC Machine Tools," International Journal of Machine Tools and Manufacture, Vol. 59, No. 8, pp. 16-23, 2012.

4. Bahk, C.-J. and Parker, R. G., "Analytical Investigation of Tooth Profile Modification Effects on Planetary Gear Dynamics," Mechanism and Machine Theory, Vol. 70, No. 6, pp. 298-319, 2013.

5. Park, D. and Kahraman, A., "A Surface Wear Model for Hypoid Gear Pairs," Wear, Vol. 267, No. 9-10, pp. 1595-1604, 2009.

6. Wang, J., Liang, H., Luo, S., and Wu, R. Y., "Active Design of Tooth Profiles Using Parabolic Curve as the Line of Action," Mechanism and Machine Theory, Vol. 67, No. 9, pp. 47-63, 2013.

7. Oh, S., Oh, S., Kang, J., Lee, I., and Lyu, S., "A study on Modeling and Optimization of Tooth Microgeometry for a Helical Gear Pair," Int. J. Precis. Eng. Manuf., Vol. 14, No. 3, pp. 423-427, 2013.

8. Li, T., Pan, C. Y., Gao, F. D., and Wang, X. C., "Research on Sliding Ratios of Conjugate Surfaces of Two Degrees of Freedom Meshing Transmission of Spherical Gear Pair," Journal of Mechanical Design, Vol. 134, No. 9, Paper No. 091002, 2012.

9. Tsai, Y.-C. and Hsu, W.-Y., "The Study on the Design of Spiral Bevel Gear Sets with Circular-Arc Contact Paths and Tooth Profiles," Mechanism and Machine Theory, Vol. 43, No. 9, pp. 1158-1174, 2008.

10. Chen, C.-F. and Tsay, C.-B., "Tooth Profile Design for the Manufacture of Helical Gear Sets with Small Numbers of Teeth," International Journal of Machine Tools and Manufacture, Vol. 45, No. 12, pp. 1531-1541, 2005.

11. Komori, T., Ariga, Y., and Nagata, S., "A New Gears Profile Having Zero Relative Curvature at Many Contact Points (Logix Tooth Profile)," Journal of Mechanical Design, Vol. 112, No. 3, pp. 430-436, 1990.

12. Chen, B. K., Liang, D., and Gao, Y. E., "The Principle of Conjugate Curves for Gear Transmission," Journal of Mechanical Engineering, Vol. 50, No. 1, pp. 130-136, 2014.

13. Chen, B. K., Gao, Y. E., and Liang, D., "Tooth Profile Generation of Conjugate-Curve Gear," Journal of Mechanical Engineering, Vol. 50, No. 3, pp. 18-24, 2014.

14. Chen, B. K. Liang, D., and Li, Z., "A Study on Geometry Design of Spiral Bevel Gears based on Conjugate Curves," Int. J. Precis. Eng. Manuf., Vol. 15, No. 3, pp. 477-482, 2014.

15. Liang, D., Chen, B. K., and Gao, Y. E., "The Generation Principle and Mathematical Model of a New Involute-Helix Gear Drive," Proceedings of the Institution of Mechanical Engineers, Part C: Journal of Mechanical Engineering Science, Vol. 227, No. 12, pp. 2834-2843, 2013.

16. Litvin, F. L. and Fuentes, A., "Gear Geometry and Applied Theory," Cambridge University Press, pp. 97-118, 2004.

17. Wu, X. T., "Principle of Gearing," Xi'An Jiaotong Unviersity Press (In Chinese), pp. 134-150, 2009.